Joint reconstruction of multiple initial pressures and the speed of sound in photoacoustic tomography

Miika Suhonen[a], Felix Lucka[b], Aki Pulkkinen[a], Simon Arridge[c], Ben Cox[d], and Tanja Tarvainen[a]

[a]University of Eastern Finland, Department of Technical Physics, Kuopio, Finland
[b]Centrum Wiskunde & Informatica, Amsterdam, The Netherlands
[c]University College London, Department of Computer Science, London, United Kingdom
[d]University College London, Department of Medical Physics and Biomedical Engineering, London, United Kingdom

ABSTRACT

The aim of the photoacoustic tomography (PAT) inverse problem is to reconstruct the initial pressure distribution from measured ultrasound waves generated by absorption of externally induced pulse of near-infrared light. Image reconstruction calls for modelling of these acoustic pressure waves, and thus knowledge of the speed of sound distribution of the target is required. However, the speed of sound is often unknown in practical situations, and therefore it would be valuable to reconstruct it together with the initial pressure. In addition, the speed of sound can provide interesting quantitative information of the imaged target. In this work, joint reconstruction of the initial pressure and speed of sound in PAT is studied. We propose an approach where photoacoustic measurements are performed using multiple different initial pressure distributions that are generated to the target using illuminations from different directions. Methodology for joint reconstruction of these multiple initial pressure and speed of sound distributions is formulated. The methodology was evaluated with numerical simulations. The results show that, utilising data generated by producing multiple initial pressures in the target, initial pressure distributions can be reconstructed more accurately with less artefacts compared to a reference approach of utilising a single light illumination.

1. INTRODUCTION

Photoacoustic tomography is an imaging modality where information about the target can be gained utilising the photoacoustic effect.[1,2] In the measurement situation, the imaged target is illuminated with a short pulse of light. Absorption of light causes pressure increase that propagates as acoustic waves to the boundary of the target, where it is measured using ultrasound sensors. Then, by performing computational image reconstruction procedure, the initial pressure in the target can be reconstructed. This reconstructed initial pressure distribution constitutes a photoacoustic image.

In the PAT computational image reconstruction, propagation of the acoustic waves needs to be modelled. The accuracy of the modelling, and therefore also the image reconstruction, relies on knowing the acoustic parameters of the target. However, these parameters are typically not known, and thus their choice, and especially the speed of sound, can affect on the reconstructed photoacoustic images significantly.[3] To reduce the artifacts due to unknown speed of sound, one can aim to select the most favorable constant speed of sound, for example by maximising the image sharpness.[4,5] Alternatively, ultrasound tomography can be utilised to reconstruct the speed of sound distribution, and that can be further utilised in PAT,[6,7] but this approach requires more complex measurement systems. Thus, it would be desirable to reconstruct the speed of sound together with the initial pressure using PAT measurements only. In addition, if the speed of sound could be reliably reconstructed from PAT data, quantitative information about the acoustic properties of the target could be gained.[8] The joint reconstruction of initial pressure and speed of sound has been shown to be ill-posed and thus difficult to solve in practise.[9,10]

Further author information: (Send correspondence to M.S.)
M.S.: E-mail: miika.suhonen@uef.fi

Photons Plus Ultrasound: Imaging and Sensing 2025, edited by Alexander A. Oraevsky, Lihong V. Wang, Proc. of SPIE Vol. 13319, 133191A · © 2025 SPIE
1605-7422 · doi: 10.1117/12.3041863

In this work, we study the joint reconstruction of initial pressure and speed of sound in PAT following the approach described in,[11] where utilising multiple initial pressure distributions to ease the ill-posedness of the problem was proposed. In this work, optical illuminations from different directions are used to create multiple different initial pressure distributions in the target. Since optical illumination does not affect to the speed of sound in the target, more information of the unknown speed of sound can be gained.

2. METHODS

2.1 Modeling the acoustic wave propagation

In an acoustically heterogeneous but non-absorbing medium, propagation of acoustic waves can be modelled with the wave equation as

$$\left(\frac{1}{c^2(r)}\frac{\partial^2}{\partial t^2} - \nabla^2\right) p(r,t) = 0, \quad r \in \mathbb{R}^d,\ t \in (0,T) \tag{1}$$

where r is the position, $c(r)$ is the speed of sound, $p(r,t)$ is the acoustic pressure at a time instance t, and d is the dimension.[2] In photoacoustic wave generation, the wave equation can be combined with initial conditions

$$p(r,t=0) = p_0(r), \quad \frac{\partial}{\partial t}p(r,t=0) = 0, \tag{2}$$

where $p_0(r)$ is the initial pressure distribution. In this work, solution of the wave equation is approximated using a k-space pseudo-spectral method that has been implemented with the k-Wave MATLAB toolbox.[12]

2.2 Joint reconstruction of the initial pressure and speed of sound

In this work, $k = 1, ..., K$ initial pressure distributions p_0^k in the target are utilised to generate a photoacoustic dataset. The PAT observation model can be written as

$$y = f(x) + e, \tag{3}$$

where y is the data, e is the additive noise in the measurements, $f(x)$ is the the forward model, and $x = \left(p_0^1, ..., p_0^K, c\right)$ are the unknown parameters of interest, i.e. initial pressure distributions p_0^k and a spatially varying speed of sound c.

Image reconstruction can be performed by minimising

$$\hat{x} = \arg\min_x \left\{ \frac{1}{2}\left\|L_e\left(y - f(x)\right)\right\|^2 + \mathcal{R}(x) \right\}, \tag{4}$$

where L_e is a weighting matrix that can be written as Cholesky factorization $L_e^\top L_e = \Gamma_e^{-1}$, where Γ_e is the covariance matrix of the noise in the measurements, and $\mathcal{R}(x)$ is the regularising penalty functional. In this work, functional

$$\mathcal{R}(x) = \frac{1}{2}\left\|L_x\left(x - \eta_x\right)\right\|^2, \tag{5}$$

is used, where η_x is the mean of the prior and $L_x^\top L_x = \Gamma_x^{-1}$ where Γ_x is the covariance matrix of the prior.

In this work, minimisation problem (4) is solved using a limited memory Broyden–Fletcher–Goldfarb–Shanno (L-BFGS) method with a backtracking line-search and bound constraints.[13] In the algorithm, the parameter vector x is updated on every iteration i as

$$x_{i+1} = \mathcal{P}\left(x_i - \alpha_i \delta_i\right), \tag{6}$$

where δ_i is the L-BFGS search direction, α_i is a step length calculated with a backtracking line search, and $\mathcal{P}$ is an operator for bound constraints. In this work, gradients of the objective function, needed to define the search direction, are calculated with an adjoint-state method.[14,15]

3. NUMERICAL SIMULATIONS

Numerical simulations were performed in a $10\,\text{mm} \times 10\,\text{mm}$ square target. The proposed approach was compared with different strategies to compensate the unknown speed of sound in the image reconstruction. The first reference approach was to use a known speed of sound distribution to reconstruct the initial pressure. This assumption can be seen as an approach that can produce the best possible outcome of the initial pressure reconstruction, but it is not realistic to do in practice. Further, a reference approach where a single initial pressure and speed of sound distributions were reconstructed simultaneously was performed. Third, we also compared the proposed approach to a situation where the speed of sound was assumed to be constant, which is an assumption that is often done in photoacoustic tomography image reconstruction. Two different values for the constant speed of sound were used. First, an "ideal" value was chosen by reconstructing multiple initial pressure distributions using different values for the speed of sound and choosing the one that maximises the sharpness of the image, see details in Ref.[5] Second, a "non-ideal" constant speed of sound was chosen arbitrarily to be within the range of typical values of the speed of sound in a soft tissue.

3.1 Data simulation

In this work, different initial pressure distributions in the target were simulated using the diffusion approximation[16] as a model for light propagation

$$\begin{cases} -\nabla \cdot \kappa(r)\nabla\Phi(r) + \mu_\text{a}(r)\Phi(r) = 0, & r \in \Omega \subset \mathbb{R}^d \\ \Phi(r) + \frac{1}{2\gamma_d}\kappa(r)\nabla\Phi(r)\cdot\hat{n} = \begin{cases} \frac{s(r)}{\gamma_d}, & r \in \epsilon \\ 0, & r \in \partial\Omega \setminus \epsilon \end{cases} \end{cases} \tag{7}$$

where $\Phi(r)$ is the photon fluence and $\kappa(r) = (d(\mu_\text{a}(r) + \mu_\text{s}'(r))^{-1}$ is the diffusion coefficient where $\mu_\text{a}(r)$ and $\mu_\text{s}'(r)$ are absorption and reduced scattering coefficients. Further, $s(r)$ is the light source at a source position $\epsilon \subset \partial\Omega$, γ_d is the dimension dependent parameter ($\gamma_2 = \frac{1}{\pi}$) and $\hat{n}$ is an outward unit normal. The initial pressure created by the photoacoustic effect can be calculated from photon fluence as

$$p_0(r) = G(r)\mu_\text{a}(r)\Phi(r), \tag{8}$$

where $G(r)$ is the Grüneisen parameter that is modelled as constant $G(r) = 1$ in this work. The solution of the diffusion approximation was numerically approximated using a finite element method where the target was discretised into a triangular grid consisting of 21402 elements and 10894 nodes. Optical parameters and the simulated fluence of light were presented in a piece-wise linear basis, and the calculated initial pressure (in the triangular grid) was linearly interpolated into 239×239 pixel grid with a pixel size of $42.0\,\mu$m. Then, photoacoustic data was numerically simulated using the wave equation in the pixel grid. For time discretisation, 1319 time points with a time step of 5.7 ns was used. In all simulations, 236 point-like acoustic detectors were located evenly on all sides of the target and 1% of noise corresponding the peak-to-peak amplitude was added to the simulated measurement data.

Two numerical phantoms were used. First numerical phantom consisted of a vessel-like structure mimicking soft-tissue, and the second one consisted of a same vessel-like structure partly surrounded by a bone-mimicking arc with a higher speed of sound. The speed of sound of sound values of 1430 m/s and 1584 m/s for background and vessel, and 2200 m/s for the bone were used. The true speed of sound parameter distributions are presented in Fig. 1 for the soft-tissue like phantom and in Fig. 2 for the phantom including a bone-like structure. Values of the optical parameters were chosen to mimic values typical of soft tissue consisting of fat and blood. Thus, the optical absorption and reduced scattering were chosen as $\mu_\text{a} = 0.002\,\text{mm}^{-1}$ and $\mu_\text{a} = 0.02\,\text{mm}^{-1}$, and $\mu_\text{s}' = 1.8\,\text{mm}^{-1}$ and $\mu_\text{s}' = 2.2\,\text{mm}^{-1}$ for background (fat) and vessel (blood), respectively. Four different initial pressure distributions were simulated by illuminating the target from each side of the target by using a planar illumination pattern. That is, initial pressure distributions p_0^1, p_0^2, p_0^3 and p_0^4 were simulated by illuminating the target from top, left, bottom and right sides of the target domain, respectively. The simulated (true) initial pressure distributions are presented in the first rows of Figs. 1 and 2. When calculating the solutions using the reference methods, where the data was simulated using only one initial pressure distribution, the initial pressure distribution p_0^1 was used.

3.2 Image reconstruction

In the image reconstruction, a different discretisation, compared to data simulation, was used to avoid the inverse crime. Furthermore, a multigrid approach was utilised, where a total of 4 different discretisations were used to avoid getting stuck into a local minimum in the iterative image reconstruction process.[11] This was carried out by reconstructing the parameters of interest in a coarse discretisation and then linearly interpolating the parameter distributions into a finer discretisation where the parameters were reconstructed. The final (finest) discretisation, where the parameters of interest were reconstructed, consisted of a 129×129 pixel grid with a pixel size of 78.1 μm. In time discretisation, 975 time points with a time step of 10.6 ns was used.

In this work, an Ornstein-Uhlenbeck prior model[17] was used as a regulariser in the solution of the minimisation problem (4). The covariance matrix of the prior can be written as $\Gamma_x = \sigma_x^2 \Xi$, where σ_x is the standard deviation of every distinct parameter distribution of x, and $\Xi_{ij} = \exp\left(-\frac{||r_i - r_j||}{\tau}\right)$ is the unit covariance matrix. In the unit covariance matrix, r_i and r_j are the pixel locations and τ defines the length of correlation between adjacent pixels. The prior parameters for each parameter were chosen so that 95% of the parameter values were expected to lie within the values of the true parameter range with mean η_x as the median of the range of the true parameter distribution. In all reconstructions, value $\tau = 0.5$ mm was used as a characteristic length scale. In addition, the noise was modelled as $\Gamma_e \sim \mathcal{N}(0, \sigma_e I)$, where the standard deviation of the noise σ_e corresponds to the true noise level of the simulated data.

When the image reconstruction was performed using a constant speed of sound, values $c = 1460$ m/s and $c = 1500$ m/s were used with the case of vessel-like target for "ideal" and "non-ideal" speed of sound values, respectively. In the case of bone-like target, values $c = 1500$ m/s and $c = 1600$ m/s were used for for "ideal" and "non-ideal" speed of sound values, respectively.

4. RESULTS

The true initial pressure and speed of sound distributions and the reconstructions are presented in Fig. 1 for the soft-tissue mimicking target. When the speed of sound is known, the reconstructed initial pressure distribution is highly accurate, as the shape of the inclusion and values of the initial pressure are close to the true parameter. With the proposed methodology, i.e. when multiple initial pressure distributions are utilised, the reconstructed initial pressure distribution resembles closely to the true parameter distributions. The reconstructed speed of sound is distorted, but the shape of the inclusion is well recognizable. In a situation, where a single initial pressure and speed of sound distributions are reconstructed simultaneously, the reconstructed initial pressure resembles the true parameter, and only small amount of artifacts are visible in the background. However, the reconstructed speed of sound is highly distorted, and the shape of the inclusion can be detected only on the bottom side of the target domain. In the case of a constant "ideal" speed of sound, the reconstructed initial pressure resembles the true parameter well. However, the reconstructed image suffers from aberrations on the background where small vessel-like artefacts are visible. If a constant, but "non-ideal" speed of sound value is used, the reconstructed initial pressure suffers highly from aberrations. In this situation, the vessel structures of the target are blurry and wider than in the true parameter.

Similar observations can be seen from the calculated relative errors that are shown in Table. 1. As expected, the calculated relative error of initial pressure p_0^1 has the smallest value when the speed of sound was known. With the proposed approach, the relative errors of p_0^1 and c are higher than with the known speed of sound, but lower than with other approaches. This confirms the visual observations that the proposed approach can provide more accurate reconstructions than the reference approaches.

The true initial pressure and speed of sound distributions and the reconstructions are presented in Fig. 2 for the target with a bone-mimicking speed of sound structure. As it could be expected, the reconstructed initial pressure, when the speed of sound was known, resembles the true parameter well. With the proposed methodology, the reconstructed initial pressure distributions resemble the true parameters: the vessel structure can be clearly distinguished and the reconstructed initial pressure values match with the true values. However, some artifacts are visible in the background. In the reconstructed speed of sound distribution, the vessel and bone structures can be distinguished but the values are notably higher in the vessel structure compared to the true parameters values. When data from a single initial pressure distribution is utilised, the reconstructed initial

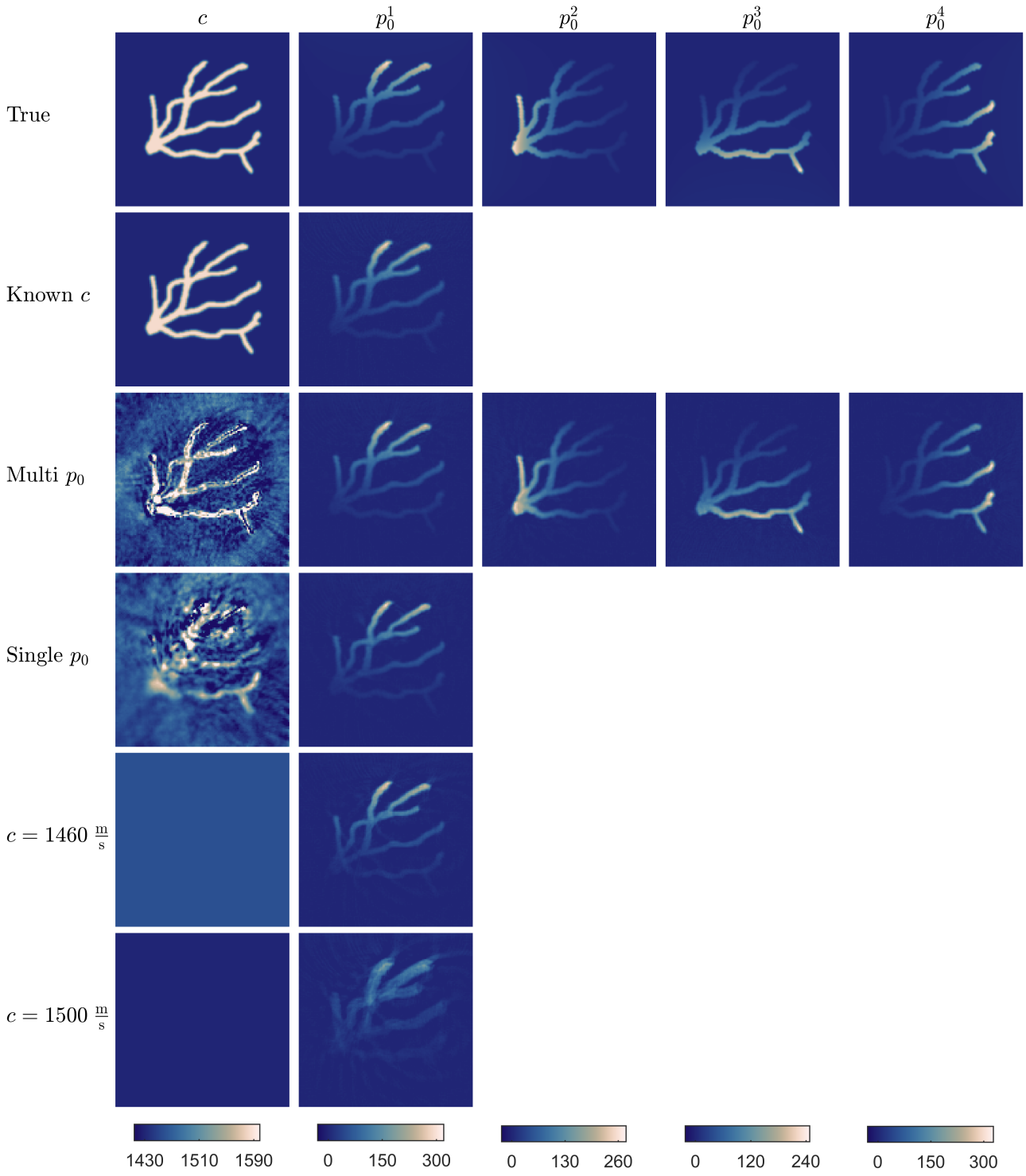

Figure 1. Reconstructed speed of sound c and initial pressure p_0^1, p_0^2, p_0^3, and p_0^4 distributions. Rows from top to bottom: simulated (true) parameters, reconstructions with a known speed of sound, reconstructions when multiple initial pressures were utilised, reconstructions when a single initial pressure was utilised, reconstructions with a constant "ideal" speed of sound, and reconstructions with a constant "non-ideal" speed of sound.

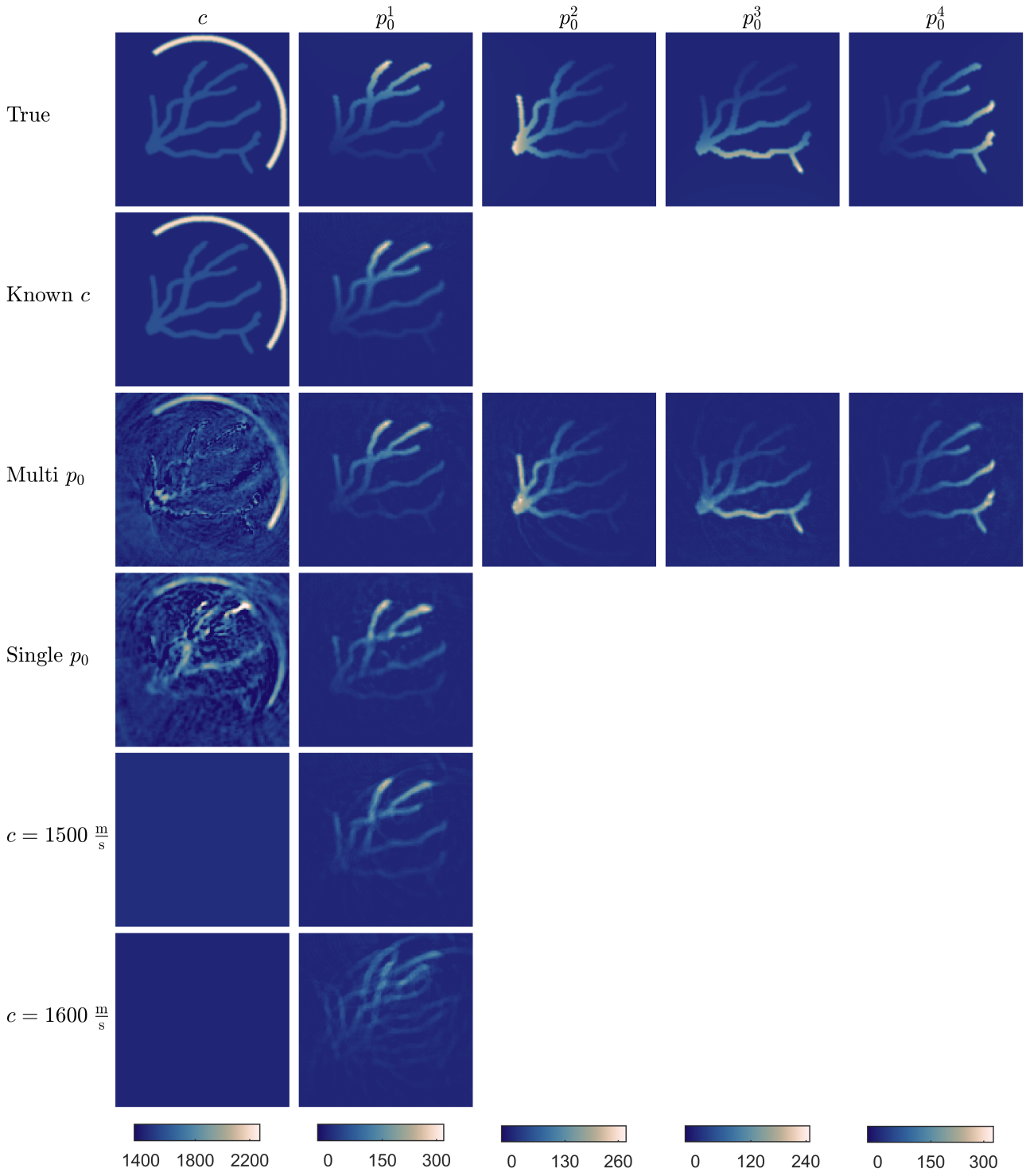

Figure 2. Reconstructed speed of sound c and initial pressure p_0^1, p_0^2, p_0^3, and p_0^4 distributions. Rows from top to bottom: simulated (true) parameters, reconstructions with a known speed of sound, reconstructions when multiple initial pressures were utilised, reconstructions when a single initial pressure was utilised, reconstructions with a constant "ideal" speed of sound, and reconstructions with a constant "non-ideal" speed of sound

Table 1. Relative errors of the reconstructed speed of sound E_c and initial pressures $E_{p_0^1}$, $E_{p_0^2}$, $E_{p_0^3}$ and $E_{p_0^4}$ distributions in different imaging scenarios.

	Vessel					Vessel and bone				
	Known c	Multi p_0	Single p_0	$c = 1460\ ^{m}/_{s}$	$c = 1500\ ^{m}/_{s}$	Known c	Multi p_0	Single p_0	$c = 1500\ ^{m}/_{s}$	$c = 1600\ ^{m}/_{s}$
$E_c(\%)$	0.0	2.9	3.3	3.1	4.7	0.0	7.2	9.2	9.8	10.2
$E_{p_0^1}(\%)$	10.2	11.7	20.4	20.0	55.4	15.6	29.4	39.3	49.4	92.4
$E_{p_0^2}(\%)$		12.8					21.1			
$E_{p_0^3}(\%)$		10.8					20.0			
$E_{p_0^4}(\%)$		10.6					26.1			

pressure resembles the true parameter distribution, but suffers from artefacts throughout the target domain. In addition, the reconstructed speed of sound is distorted and the shape of the vessel is not clear. On the other hand, the curved bone-like structure can be distinguished. The reconstructed initial pressure in the case of a constant "ideal" speed of sound resembles the true distribution, but suffers from aberrations especially in the background where the vessel-like artefacts are visible. In the case of a constant but "non-ideal" speed of sound, the reconstructed initial pressure suffers highly from aberrations and the vessel structure can not be distinguished.

From the calculated relative errors (Table. 1) we can see that the relative error for the initial pressure is lowest when the speed of sound was known, as could be expected. With the proposed approach, the relative errors of p_0^1 and c are lower compared to other approaches. The relative errors of the speed of sound and initial pressure are lower when a single initial pressure and speed of sound are reconstructed jointly, compared of assuming the speed of sound as a constant. These relative error values, together with the visual observations, indicate that the image reconstruction accuracy can be enhanced when the speed of sound is reconstructed with the initial pressure compared to using a constant speed of sound value to reconstruct the initial pressure. Further, the accuracy can be even further improved by utilising the proposed approach of using multiple initial pressures.

5. CONCLUSIONS

In this work, a joint reconstruction of initial pressure and the speed of sound in PAT was studied. We proposed a methodology that utilised a dataset of multiple initial pressure distributions generated by illuminations from different directions. Then, these different initial pressure distributions were reconstructed together with the speed of sound distribution. The results show that the approach can lead to an enhanced image quality when compared to an approach of reconstructing a single initial pressure and speed of sound distributions simultaneously, or to an approach where the initial pressure distribution is reconstructed by assuming a constant speed of sound in the target.

ACKNOWLEDGMENTS

This project was supported by the European Research Council (ERC) under the European Union's Horizon 2020 research and innovation programme (grant agreement No 101001417 - QUANTOM) and by the Research Council of Finland (Centre of Excellence in Inverse Modelling and Imaging grant 353086, Flagship of Advanced Mathematics for Sensing Imaging and Modelling grant 358944), Finnish Cultural Foundation (South Savo Regional Fund), and Magnus Ehrnrooth Foundation. B.C. acknowledges the support of the Engineering and Physical Sciences Research Council, UK (EP/W029324/1, EP/T014369/1).

REFERENCES

[1] Beard, P., "Biomedical photoacoustic imaging," *Interface Focus* **1**, 602–631 (2011).

[2] Li, C. and Wang, L., "Photoacoustic tomography and sensing in biomedicine," *Physics in Medicine and Biology* **54**(19), R59–R97 (2009).

[3] Wang, T., Liu, W., and Tian, C., "Combating acoustic heterogeneity in photoacoustic computed tomography: A review," *Journal of Innovative Optical Health Sciences* **13**(3), 2030007 (2020).

[4] Mandal, S., Nasonova, E., Dean-Ben, X., and Razansky, D., "Optimal self-calibration of tomographic reconstruction parameters in whole-body small animal optoacoustic imaging," *Photoacoustics* **2**, 128–136 (2014).

[5] Treeby, B., Varslot, T., Zhang, E., Laufer, J., and Beard, P., "Automatic sound speed selection in photoacoustic image reconstruction using an autofocus approach," *Journal of Biomedical Optics* **16**(9), 090501 (2011).

[6] Jose, J., Willemink, R., Steenbergen, W., Slump, C., van Leeuwen, T., and Manohar, S., "Speed-of-sound compensated photoacoustic tomography for accurate imaging," *Medical Physics* **32**(12), 7262–7271 (2012).

[7] Matthews, T. and Anastasio, M., "Joint reconstruction of the initial pressure and speed of sound distributions from combined photoacoustic and ultrasound tomography measurements," *Inverse Problems* **33**, 124002 (2017).

[8] Li, C., Duric, N., Littrup, P., and Huang, L., "*In vivo* breast sound-speed imaging with ultrasound tomography," *Ultrasound in Medicine & Biology* **35**(10), 1615–1628 (2009).

[9] Huang, C., Wang, K., Schoonover, R., Wang, L., and Anastasio, M., "Joint reconstruction of absorbed optical energy density and sound speed distributions in photoacoustic computed tomography: A numerical investigation," *IEEE Transactions on Computational Imaging* **2**(2), 136–149 (2016).

[10] Stefanov, P. and Uhlmann, G., "Instability of the linearized problem in multiwave tomography of recovery both the source and the speed," *Inverse Problems and Imaging* **7**(4), 1367–1377 (2013).

[11] Suhonen, M., Lucka, F., Pulkkinen, A., Arridge, S., Cox, B., and Tarvainen, T., "Reconstructing initial pressure and speed of sound distributions simultaneously in photoacoustic tomography," Manuscript in preparation (2025).

[12] Treeby, B. and Cox, B., "k-wave: MATLAB toolbox for the simulation and reconstruction of photoacoustic wave fields," *Journal of Biomedical Optics* **15**(2), 021314 (2010).

[13] Nocedal, J. and Wright, S., [*Numerical Optimization*], Springer Nature (2006).

[14] Arridge, S., Betcke, M., Cox, B., Lucka, F., and Treeby, B., "On the adjoint operator in photoacoustic tomography," *Inverse Problems* **32**(11), 115012 (2016).

[15] Bunks, C., Saleck, F., Zaleski, S., and Chavent, G., "Multiscale seismic waveform inversion," *Geophysics* **60**(5), 1457–1473 (1995).

[16] Tarvainen, T., Cox, B., Kaipio, J., and Arridge, S., "Reconstructing absorption and scattering distributions in quantitative photoacoustic tomography," *Inverse Problems* **28**(11), 084009 (2012).

[17] Rasmussen, C. and Williams, C., [*Gaussian Processes for Machine Learning*], Cambridge, MA, USA: MIT Press (2006).